

Critical Analysis of Glass Stability Parameters and Application to Lithium Borate Glasses

Eduardo B. Ferreira,[‡] Edgar D. Zanotto,^{§,†,*} Steve Feller,^{¶,*,**} Grant Lodden,[¶] Joy Banerjee,[¶] Trent Edwards,[¶] and Mario Affatigato^{¶,*,**}

[‡]Department of Materials Engineering, University of Sao Paulo, Sao Carlos, 13566-590, Brazil

[§]DEMa/LaMaV – Vitreous Materials Laboratory, Federal University of Sao Carlos, Sao Carlos, 13565-905, Brazil

[¶]Physics Department, Coe College, Cedar Rapids, IA 52402

We reevaluated nine parameters of glass stability (GS) against crystallization determined from differential scanning calorimetry (DSC) experiments to predict the glass-forming ability (GFA) of oxide liquids on cooling. Then, borate glasses were prepared and tested, covering the $\text{Li}_2\text{O}-\text{B}_2\text{O}_3$ system with 20.0–66.7 mol% lithia. The glasses were prepared from both commercial chemical and powders, obtained by a solution method. The GS parameters were calculated using characteristic glass transition, crystallization, and melting peaks of DSC thermograms. We found that seven stability parameters give similar trends for compositions up to 33.3 mol% lithia, where, as we expected, GS significantly decreases with lithia content. Thereafter, up to 66.7 mol% lithia, GS shows a broad shallow maximum, but is approximately constant indicating that, surprisingly, composition does not significantly affect the GFA in this wide compositional range. This result qualitatively agrees with our successful experience of preparing glasses with compositions up to 74 mol% lithia and corroborates the adequacy of simple DSC tests to comparatively gauge the GS and GFA of glass-forming liquids.

I. Introduction

NEW glasses for specific applications have enormous technological interest. An estimate of the possible number of glasses to be synthesized by 1% combinations of up to 80 “friendly” elements of the periodical table exceeds 10^{50} compositions, whereas in the last 6000 years of glass history, less than 10^6 glasses have been reported!¹ In addition, most existing glasses have only 1–10 elements in their composition. Therefore, a practically infinite number of exciting new compositions could be vitrified and their properties tested, for instance by combinations of up to 80 elements.

The development of new glass compositions, the range within which a process must be controlled to produce a glass, or to which direction certain compositions could be altered to improve their vitrification ability, for example, are of paramount importance for the glass technologist. However, despite deeper understanding in the last few decades, it is still a great challenge to quantitate the ease with which a given

composition will not crystallize and vitrify on cooling from the liquid state.

For a frozen liquid to be considered a glass, the crystallized fraction must not exceed the experimental limit of detection, say $X_c = 10^{-3}$. In his classical papers on the kinetics of glass formation, Uhlmann, Ref. [2], assumed 10^{-6} as a typical figure for the limit of detection. Here, we assume a practical limit of 10^{-3} (0.1%) because this value is much closer to the real experimental limit of detection of X-ray diffraction (XRD), small-angle X-ray scattering (SAXS), or nuclear magnetic resonance (NMR), for instance. A direct measurement of the glass-forming ability (GFA) of any material is thus the critical cooling rate at which the melt must be cooled to yield a crystallized fraction below this limit.² Hence, the higher the critical cooling rate, the more difficult it is to obtain a glass, or the lower is the GFA of that composition.

However, there are several difficulties in measuring the critical cooling rate. Many compositions crystallize far too fast, being difficult to monitor any change in their vitrification behavior with changes in composition or in process parameters. Nor it is easy to continuously vary the cooling rate. Approximately, from 1 to 50°C/min, the cooling rate can be precisely controlled and recorded in laboratory furnaces. Lower cooling rates (<1°C/min) are still possible to control, but the experiments take a long time, the crystallized fraction can sometimes be too low for detection and the whole procedure ends up being very time consuming. On the other hand, faster cooling rates (>50°C/min) are quite feasible but not easy to be controlled due to the thermal inertia of most furnaces. In general, high cooling rates are obtained by quenching a liquid into some fluid, such as, oil or water. However, intermediate rates are not always possible. Alternatively, molten liquids can be efficiently cooled in contact with cold substrates with high thermal conductivity, for example, graphite or some metal. In such processes, the liquid can be pressed at different rates (e.g., splat cooling) or poured on a moving substrate (e.g., melt spinning). One can measure the temperature throughout the process, but it is not trivial to achieve and to control some desired cooling rate.

In addition, the crystallized fraction in partially transformed materials (when a liquid solidifies as a glass) is not always easy to quantitate. Traditionally, crystals are observed in polished sections of the material by optical or electron microscopy. The quantitative characterization of the crystallized volume fraction involves the suitable preparation of many samples and individual analysis under a microscope is tedious, time consuming, and restricted by the resolution limit of the equipment. Instrumental detection of the crystallized fraction is also possible, for example, by XRD techniques, but this requires sophisticated devices, fine sam-

L. Pinckney—contributing editor

Manuscript No. 29717. Received May 11, 2011; approved June 29, 2011.

This work was presented at the XXII International Congress on Glass, Salvador, Brazil, September 24, 2010 (Oral Section A, Presentation 363, www.icg2010.com.br).

This work was supported by the NSF (USA), under Grants No. DMR-05020518 and DMR-0904615, Fapesp (Brazil) 07/008179-9 and CNPq (Brazil).

*Member, The American Ceramic Society

**Fellow, The American Ceramic Society

†Author to whom correspondence should be addressed. e-mail: dedz@ufscar.br.

ple preparation and expert analysis, which are not always available for a multiple-sample experimental design.

The critical cooling rate to avoid a certain minimal crystallized fraction can be estimated by theory according to several methods. One of the most widely accepted is the “nose method” based on *temperature–time–transformation* (TTT) curves, for isothermal experiments, or their counterpart *continuous cooling–transformation* (CCT) curves, for non-isothermal cooling.² However, the parameters needed for such calculations, such as the crystal nucleation and crystal growth rates, or the parameters to calculate these quantities (surface energy, thermodynamic driving force, and diffusivities) are not trivial to obtain, and are only available for a very few simple systems. In general, commercial compositions with many components are far too complex for a theoretical estimation of its phase transformation kinetics.

This scenario leads to a search for new methods of evaluation of the glass-forming ability. Such methods are indirect and mostly empirical, and their correlation with more realistic parameters, such as the critical cooling rate have been a focus of discussion in the current literature.³ For instance, Nascimento *et al.*⁴ tested nine glass stability parameters (GS) by comparing them with the critical cooling rates (q_{cr}) of several glasses that undergo preferential surface crystallization. The critical cooling rates were calculated from the experimentally obtained crystallization kinetics of the tested glasses, whereas the GS parameters were calculated from simple algebraic relations between the characteristic temperatures obtained from differential scanning calorimetry (DSC) traces: the glass transition temperature (T_g), the onset temperature of the crystallization peak on heating (T_x), the maximum of the crystallization peak (T_c), and the melting (or liquidus) point (T_m). Table I shows the nine GS parameters tested in Ref. [4]. Those authors concluded that only three of the nine parameters (K_W , K_H , and K_{LL} , see Table I) show good correlations with q_{cr} .

The aim of the present study was to further test the adequacy of the same nine stability parameters analyzed in Ref. [4] to predict glass-forming ability. For such tests, we choose several Li–B–O glasses covering a wide range of compositions across the Li_2O – B_2O_3 phase equilibrium diagram and evaluated GS as a function of composition, from (supposedly) reluctant glass-forming compositions, with mol% lithia as high as 66.7, to very good glass-forming compositions with 20.0 mol% lithia.

Furthermore, these glasses have been well studied by a host of spectroscopic techniques (NMR, Raman, Infrared, etc.).^{11–14} The structures, both short and intermediate range, have been characterized over several decades (see end of discussion for details).

Table I. Glass Stability Parameters (Temperatures in K)

	Source: authors and references	Equation number
$K_{LL} = \frac{T_x}{T_g + T_m}$	Lu & Liu ^{5,6}	(1)
$K_H = \frac{T_x - T_g}{T_m - T_x}$	Hruby ⁷	(2)
$K_W = \frac{T_x - T_g}{T_m}$	Weinberg ⁸	(3)
$K_T = \frac{T_g}{T_m}$	Turnbull ⁹	(4)
$K_{SP} = \frac{(T_x - T_g)(T_c - T_x)}{T_g}$	Saad and Poulain ¹⁰	(5)
$K_1 = T_m - T_g$	In: Nascimento <i>et al.</i> ⁴	(6)
$K_2 = T_x - T_g$	In: Nascimento <i>et al.</i> ⁴	(7)
$K_3 = \frac{T_x}{T_m}$	In: Nascimento <i>et al.</i> ⁴	(8)
$K_4 = \frac{(T_x - T_g)(T_c - T_x)}{T_m}$	In: Nascimento <i>et al.</i> ⁴	(9)

II. Experimental Procedure

The glasses were prepared using two procedures. In the conventional melt method high purity lithium carbonate and boric acid powders were mixed together thoroughly and heated at 1000°C for 20–25 min. A weight loss after an initial 15–20 min of heating confirmed the sample composition to within a few percent of the nominal value. We term this, the *carbonate method* (CM). In the *solution method* (SM),¹⁵ aqueous solutions of boric acid and lithium hydroxide were reacted at room temperature. The resulting precipitate was heated to 1000°C to form the glass.

The compositions prepared for the present study are indicated in the phase equilibrium diagram (PED)¹⁶ of Fig. 1, with $R = n_{\text{Li}_2\text{O}}/n_{\text{B}_2\text{O}_3}$, where $n_{\text{Li}_2\text{O}}$ and $n_{\text{B}_2\text{O}_3}$ are the corresponding Li_2O and B_2O_3 mole number, respectively. These samples are referred to as R0.25 for $R = 0.25$, R0.5 for $R = 0.5$, and so on. Sample details are given in the Table II.

After melting and forming, the glasses were stored into closed pots with silica gel to avoid the attack of the atmosphere moisture. The samples for DSC studies were prepared immediately before each analysis by crushing the glasses in an agate mortar and pestle, in a moisture minimized environment by letting an air conditioner and a dehumidifier permanently turned on. Samples showing signs of devitrification were carefully inspected to gather only glassy pieces to be ground. The particles were collected between 38 and 22 μm sieves. The sample mass was 20.0 mg for all analyses. The thermal analyses were carried out at 10°C/min on heating and on cooling in a DSC (Model 404, NETZSCH-Gerätebau GmbH, Selb, Germany) at LaMaV-UFSCar.

III. Results and Discussion

The DSC traces for each composition are shown in Figs. 2–9. The important characteristic temperatures are indicated in each DSC trace and are summarized in Table III.

All compositions present typical glass transition and crystallization peaks easy to recognize in the DSC traces. The fine powders (22–38 μm) were chosen to guarantee that the DSC crystallization peaks were mainly due to surface crystallization, relegating internal crystallization, if present, to a less important secondary phenomenon, in this particular case.

The analysis of the DSC melting peaks is not as simple as that for the crystallization peaks. On heating DSC traces of the two R0.25 samples (Fig. 2), there is a first exothermic peak above T_g , which is a sign of crystallization, followed by two endothermic peaks with an intermediate exothermic sign between them. Such peaks apparently do not have any

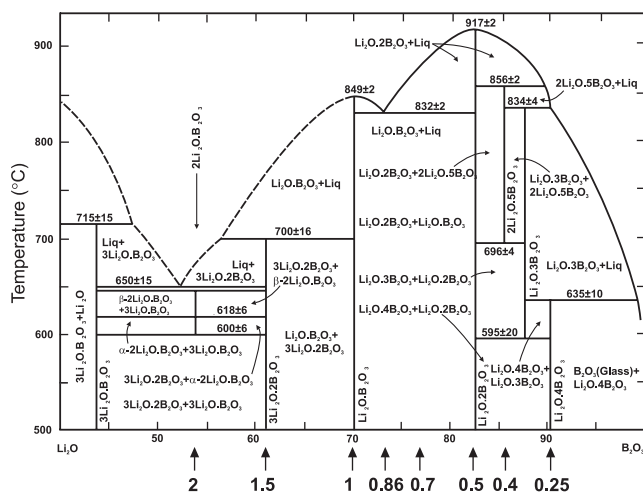
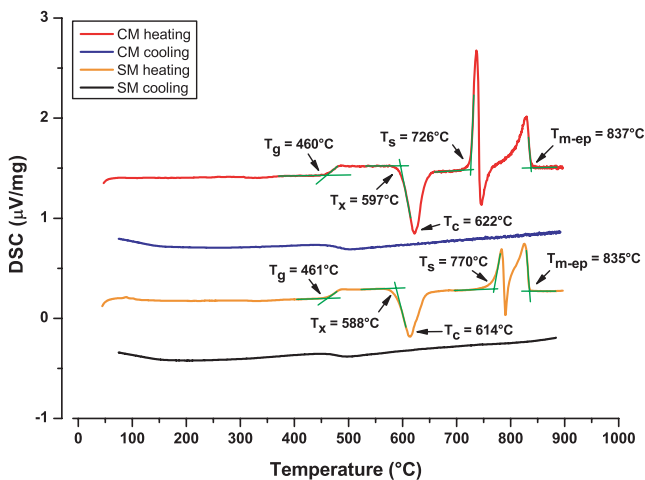
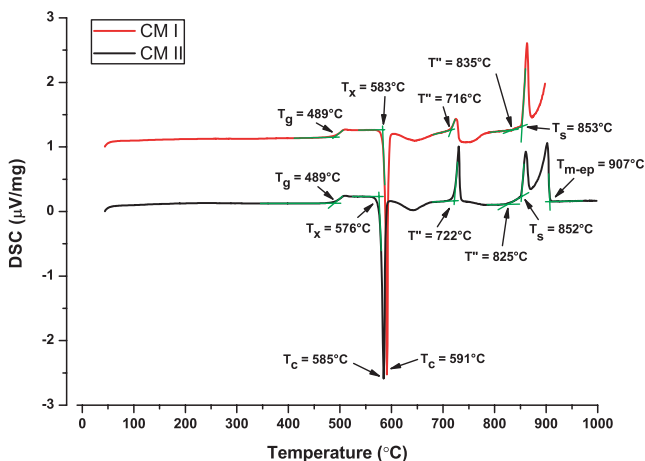


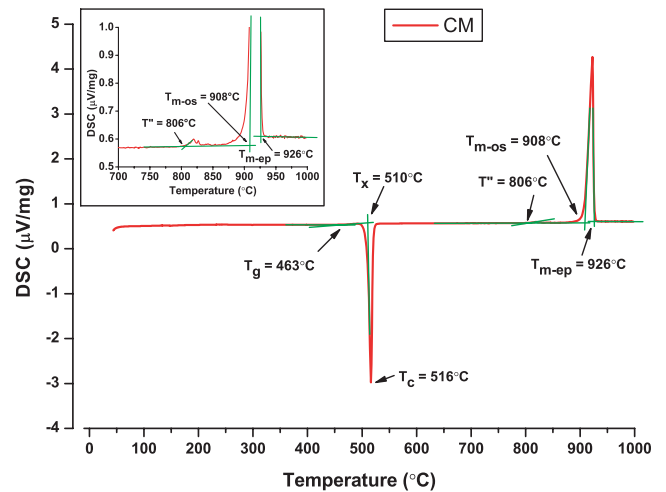
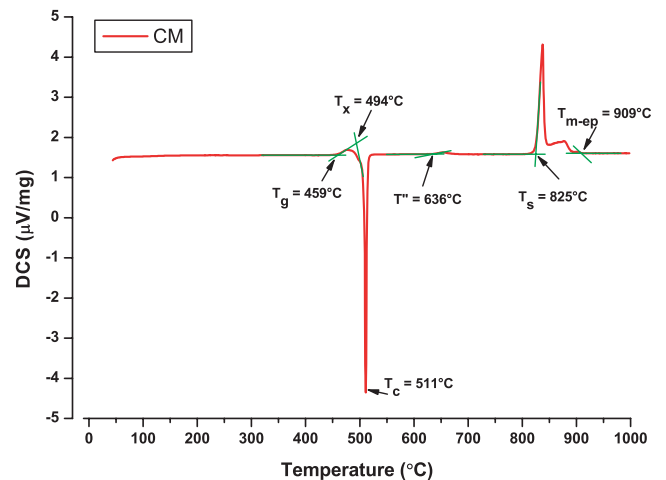
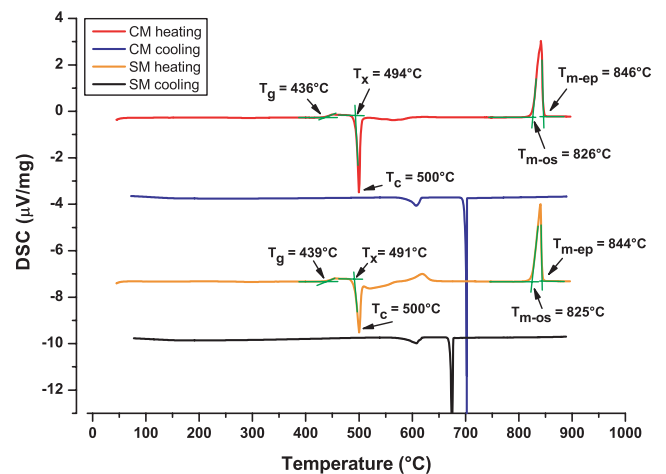
Fig. 1. Li_2O – B_2O_3 equilibrium phase diagram (wt%),¹⁶ temperatures in °C. The arrows indicate the $\text{Li}_2\text{O}/\text{B}_2\text{O}_3$ mol ratios of all compositions tested in this study.

Table II. Sample Characteristics of Different Glasses

$R = n\text{Li}_2\text{O}/n\text{B}_2\text{O}_3$ (mol ratio)	mol% Li_2O	Method	Sample shaping
0.25	20.0	Carbonate	Bulk drops
0.25	20.0	Solution	Pieces
0.4	28.6	Carbonate	Roller quenched
0.5	33.3	Carbonate	Roller quenched
0.7	41.2	Carbonate	Roller quenched
0.86	46.2	Carbonate	Roller quenched
0.86	46.2	Solution	Roller quenched
1.0	50.0	Carbonate	Roller quenched
1.0	50.0	Solution	Roller quenched
1.0 (replica)	50.0	Solution	Roller quenched
1.5	60.0	Carbonate	Roller quenched
2.0	66.7	Carbonate	Roller quenched
2.0	66.7	Solution	Roller quenched
2.0 (replica)	66.7	Solution	Roller quenched

**Fig. 2.** DSC traces of R0.25 glass (20.0 mol% Li_2O). CM, carbonate method; SM, solution method.**Fig. 3.** DSC traces of glass with $R = 0.4$ (28.6 mol% Li_2O). CM, carbonate method; SM, solution method. (I and II here are repetitions of the DSC analysis.)

correlation with the temperatures of phase transition in the published PED (Fig. 1). A possible explanation is that, due to its high B_2O_3 content, the R0.25 sample presents slow kinetics of phase transformation and does not reach equilibrium at relatively low temperatures, and thus the corresponding reaction at the solidus temperature is delayed in a non-isothermal DSC analysis, only occurring at 726°C–770°C,

**Fig. 4.** DSC traces of glass with $R = 0.5$ (33.3 mol% Li_2O). CM, carbonate method; SM, solution method.**Fig. 5.** DSC traces of glass with $R = 0.7$ (41.2 mol% Li_2O). CM, carbonate method; SM, solution method.**Fig. 6.** DSC traces of glass with $R = 0.86$ (46.2 mol% Li_2O). CM, carbonate method; SM, solution method.

that is, above the equilibrium *solidus* (635°C) (Fig. 1). At higher temperatures, the kinetics is accelerated and melting in non-isothermal analyses (835°C–837°C) completes closer to the equilibrium temperature (834°C). One may

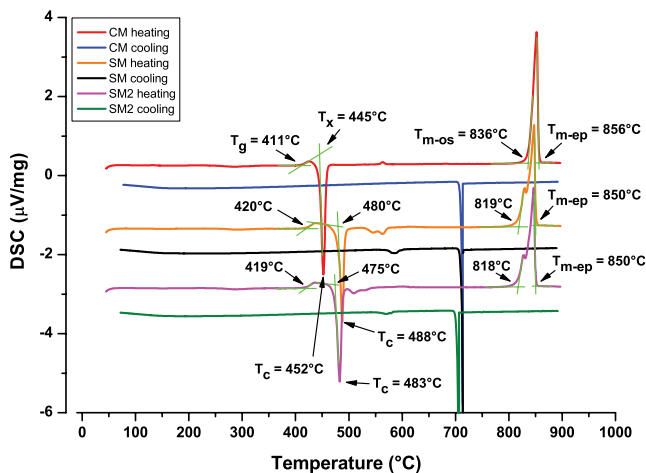


Fig. 7. DSC traces of glass with $R = 1.00$ (50.0 mol% Li_2O). CM, carbonate method; SM, solution method.

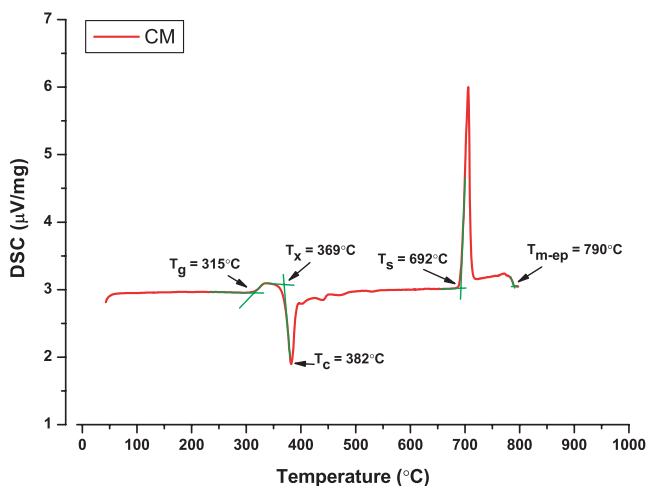


Fig. 8. DSC traces of glass with $R = 1.5$ (60.0 mol% Li_2O). CM, carbonate method; SM, solution method.

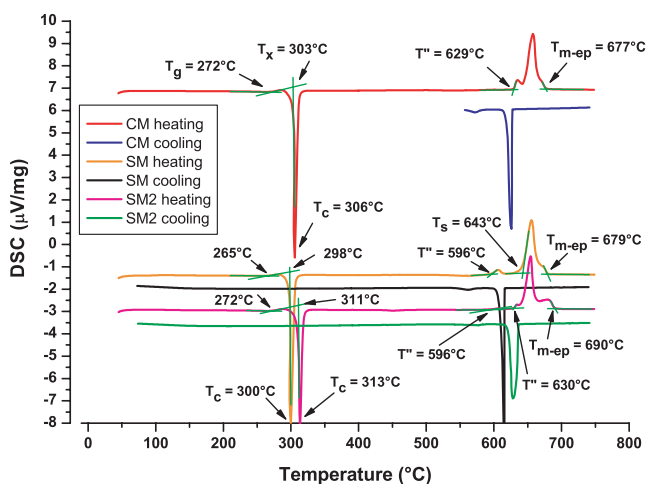


Fig. 9. DSC traces of glass with $R = 2.00$ (66.7 mol% Li_2O). CM, carbonate method; SM, solution method.

argue that the *liquidus* of the PED¹⁶ has some error by itself. It is also worth mentioning that non-isothermal DSC analyses do not guarantee that the detected melting peaks refer to the equilibrium phases. Nevertheless, on heating, the endpoint of the last endothermic peak (average 836°C) is very close to the *liquidus* indicated by the PED (834°C). An

error of about 10°C in the *liquidus*¹⁷ can be attributed to the non-zero heating rate. Only the glass transition (no crystallization) is observed for the R0.25 composition on the cooling path from the melt corroborating its good glass-forming ability. The T_g , T_x , T_c , and T_m used in our calculations are most likely not significantly affected by the intermediary reactions between 726°C and 800°C.

The characteristic temperatures in the DSC thermograms of Figs. 2–9 are summarized in Table III. For non-eutectic or non-congruent-melting compositions, except for R0.25 in Table III, one may observe that the *solidus* temperature (T_s) is estimated by the onset of the melting peak, compared with the *solidus* of the corresponding compositions in the phase equilibrium diagram (Fig. 1).

It is worth noting that the onset of the DSC melting peak (T_{m-os}) gives the best estimate for the *liquidus* temperature (T_l) for congruent-melting or eutectic compositions, that is, an estimate of the first sign of the sharp melting of such compositions.¹⁷ This is true for samples R1.0, R0.86, and R0.5. On the other hand, for non-congruent melting and non-eutectic compositions, melting occurs in a wide temperature range, and its end (the *liquidus* temperature) is thus closer to the DSC melting endpoint (T_{m-ep}), as thoroughly discussed in Ref. [17], and this is the case for samples R2.0, R1.5, R0.7, R0.4, and R0.25.

The *liquidus* temperatures, measured by DSC, of all compositions more or less agree with the corresponding reported *liquidus*,¹⁶ as shown in Fig. 10. For compositions that are non-stoichiometric or having non-congruent melting, i.e., R2.0, R1.5, R0.7, R0.4, and R0.25, the obtained *liquidus* were between 1°C and 30°C above the *liquidus* of the literature phase diagram. For compositions that are eutectic or having a congruent melting (R1.0, R0.86 and R0.5), the DSC *liquidus* were between 9°C and 11°C below the *liquidus* of the phase diagram. It is possible to argue that the positive heating rate affects the DSC characteristic temperatures. Indeed, one can expect a deviation of ~10°C in the endpoint temperature of the DSC melting peak if the heating rate is extrapolated to 0°C/min.¹⁷ However, it is reasonable to admit an approximately constant deviation for all compositions due to the non-null heating rate.¹⁷ Then the parameters calculated by the equations in Table I would also be shifted by a similar constant factor, not significantly affecting their relationship with R . To calculate the GS parameters (Table I), we used the characteristic temperatures of Table III. The onset of the DSC melting peak (T_{m-os}) was used for samples R1.0, R0.86, and R0.5, and the DSC melting endpoint (T_{m-ep}) was used for samples R2.0, R1.5, R0.7, R0.4, and R0.25.

To test the proposed GS methods, first, we carefully recalculated the nine GS parameters using data from Nascimento *et al.*⁴ and plotted them as a function of the critical cooling rates (q_{cr}) calculated in Ref. [4] for the different glasses: GeO_2 (G), $\text{PbO}\cdot\text{SiO}_2$ (PS), $\text{Na}_2\text{O}\cdot 2\text{SiO}_2$ (NS2), $2\text{MgO}\cdot 2\text{Al}_2\text{O}_3\cdot 5\text{SiO}_2$ (M2A2S5), $\text{Li}_2\text{O}\cdot 2\text{SiO}_2$ (LS2), $\text{CaO}\cdot\text{MgO}\cdot 2\text{SiO}_2$ (CMS2), $\text{CaO}\cdot\text{Al}_2\text{O}_3\cdot 2\text{SiO}_2$ (CAS2), $\text{Li}_2\text{O}\cdot 2\text{B}_2\text{O}_3$ (LB2). To facilitate our following analysis, the results are shown on the left hand side of Figs. 11–19.

The limit of detection of crystallinity is more or less arbitrary, generally taken somewhat below the real limit of detection of the equipment used to probe the presence of crystalline phases, for example, XRD. Approximately, 10^{-3} (0.1%) crystallized fraction (X_c), the value used in Ref. [4], was based on the authors' experience. But the calculated critical cooling rate (q_{cr}) depends only weakly on this value. Hence, if a lower value of X_c was used, this would equally shift the values of q_{cr} for all glasses by the same amount. Thus, the use of any other reasonable value of X_c would not affect our conclusions.

There are relative errors of ~10% in q_{cr} due to an assumed typical error of 10% in the experimental growth rates, $u(T)$, which were used for the calculations of q_{cr} . But such errors

Table III. Characteristic Temperatures (°C) from the DSC Traces of Figs. 2–9.

<i>R</i>	mol% Li ₂ O	Method	<i>T_g</i>	<i>T_x</i>	<i>T_c</i>	<i>T^m</i>	<i>T_s</i> PED ¹⁶	<i>T_{m-os}</i>	<i>T_{m-ep}</i>	<i>T₁</i> PED ¹⁶	
0.25	20.0	Carbonate	460	597	622	<i>T_s</i> = 726 [‡]	635 ± 10	–	–	835	
		Solution	461	588	614	<i>T_s</i> = 770 [‡]					
0.4	28.6	Carbonate	489	583	591	716	856 ± 2	–	–	905	
			835	<i>T_s</i> = 853							
			489	576	585	722					825
0.5 [†]	33.3	Carbonate	463	510	516	806	–	908	926	917 ± 2	
0.7	41.2	Carbonate	459	494	511	636	832 ± 2	–	909	879	
0.86 [†]	46.2	Carbonate	436	494	500	–	–	826	846	832 ± 2	
		Solution	439	491	500	–	–	825	844		
1.0 [†]	50.0	Carbonate	411	445	452	–	–	836	856	849 ± 2	
		Solution I	420	480	488	–	–	819	850		
		Solution II	420	475	483	–	–	818	850		
1.5	60.0	Carbonate	315	369	382	<i>T_s</i> = 692	700 ± 16	–	790	768	
2.0	66.7	Carbonate	272	303	306	629 [‡]	650 ± 15	–	–	677	673
		Solution I	265	298	300	596					
		Solution II	272	311	313	596					

[†]stoichiometric and eutectic compositions: *T_{m-os}*–*T₁* PED as concluded in Ref. [17].
[‡]*T^m* worth mentioning temperatures.

[‡]some experimental uncertainty in the determination of solidus temperature *T_s*.
The estimated precision of the DSC temperatures is ±3°C–5°C.

I and II are replica of the same experimental set.

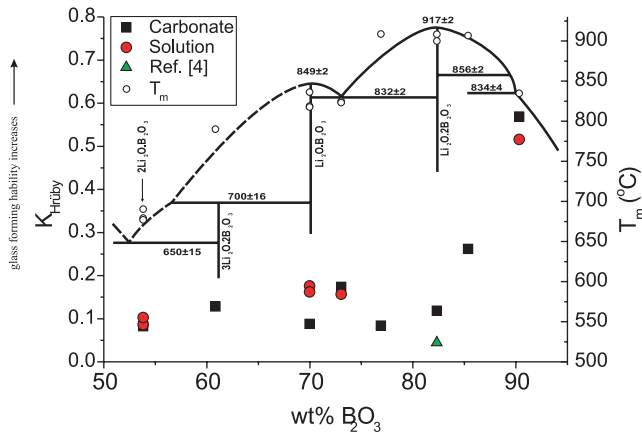


Fig. 10. Liquidus temperature, *T_m*, of different compositions in the system Li₂O–B₂O₃ obtained by DSC (open circles) compared with the liquidus temperatures of a phase diagram from Ref. [16]. The error in *T_m* is smaller than the size of the data point (±5°C). In the same graph, *K_H* is shown for the same compositions. The errors in *K_H* are shown in Fig. 12.

are smaller than the data points in the log scale of Figs. 11–19. For the calculations of *q_{cr}*, the number of nucleation sites per unit surface area, *N_s*, was considered constant (10⁴ m⁻²) and equal for all undercooled liquids, thus it does not contribute to the estimated errors.

We recall that the calculated critical cooling rates of this article refer to surface nucleation. Hence, the two glasses that also present internal nucleation in addition to surface nucleation (LS2 and LB2) could lead to a deviation of the data points in the graphs on the left hand side of Figs. 11–19. Indeed, although some GS points relative of these two compounds are quite close to the line fits of Figs. 11–19, when they deviate, for example, LS2 in Figs. 11, 12, and 18, the shift direction may indicate some additional nucleation, which would lead to a smaller *T_x*, and consequently, to a

smaller GS than expected if only surface nucleation was present. But, in general, the effect of internal nucleation in these two glasses was negligible compared to copious surface nucleation of the fine powders used here.

Our careful review of critical cooling rates and GS calculations led us to observe that possibly seven of the nine GS parameters considered in Ref. [4], that is, *K_{LL}*, *K_H*, *K_W*, *K_{SP}*, *K₂*, *K₄*, and *K₃* (and not only the first three) show some correlation with the cooling rate. But, in agreement with Ref. [4], *K_{LL}*, *K_H*, and *K_W* visually yield much better correlations and thus, should be preferentially used when the three DSC characteristic temperatures are available.

We must point out that the choice of linear regressions in the graphs in the left hand side of Figs. 11–19 is arbitrary, based on the general trend apparently shown by most of the data points. However, there is no physical reason for that choice. Indeed, one could, for instance, fit a high-order polynomial to the data of left hand side Figs. 15 and 19, and achieve higher correlation coefficients. Linear regressions were chosen for their simplicity and a guide to the eye.

Figure 20 compares the four GS parameters that scale in a similar range. One can see that among *K_{LL}*, *K_H*, *K_W*, and *K₃*, *K_H* covers the widest range, thus being the most stable against statistical errors in the determination of the characteristic temperatures by DSC. This conclusion agrees with the recent theoretical calculations of Kozmidis-Petrovic.¹⁸

The GFA estimated by most of the tested GS parameters allows one to qualitatively compare the ease with which a certain composition can be obtained as a glass in comparison to the others. This is an important tool when one aims, for instance, to optimize the GFA by varying the composition within a given system, although the time period needed for significant crystallization at any temperature, and the critical cooling rate are the most relevant parameters to be determined.

The GFA estimated by the GS parameters from DSC experiments can be used for systems for which crystallization is fast enough to be detected in dynamic, non-isothermal tests, such as the DSC. But as the best GS parameters

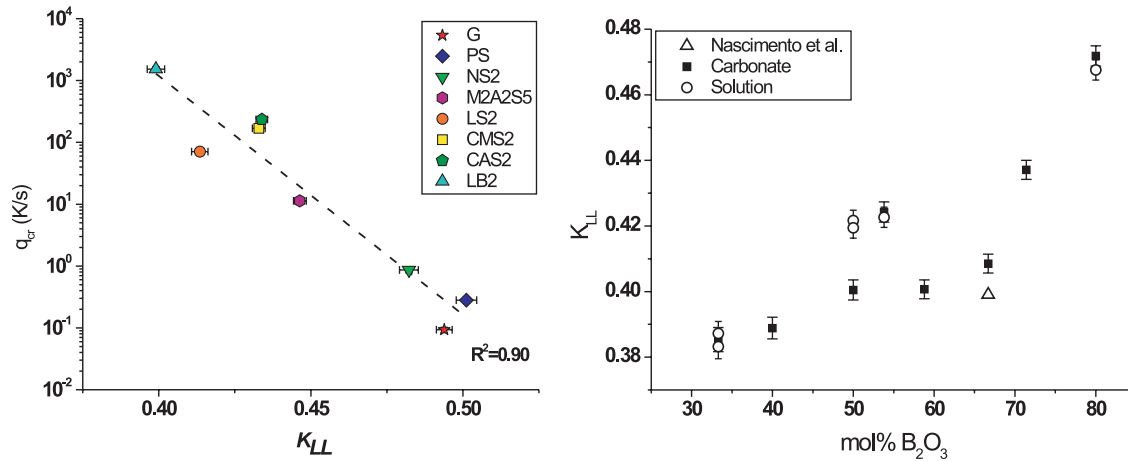


Fig. 11. Left: critical cooling rate⁴ versus the glass stability parameter $K_{LL} = T_x / (T_g + T_m)$ for several compositions. Right: the same K_{LL} versus composition in the Li_2O – B_2O_3 system.

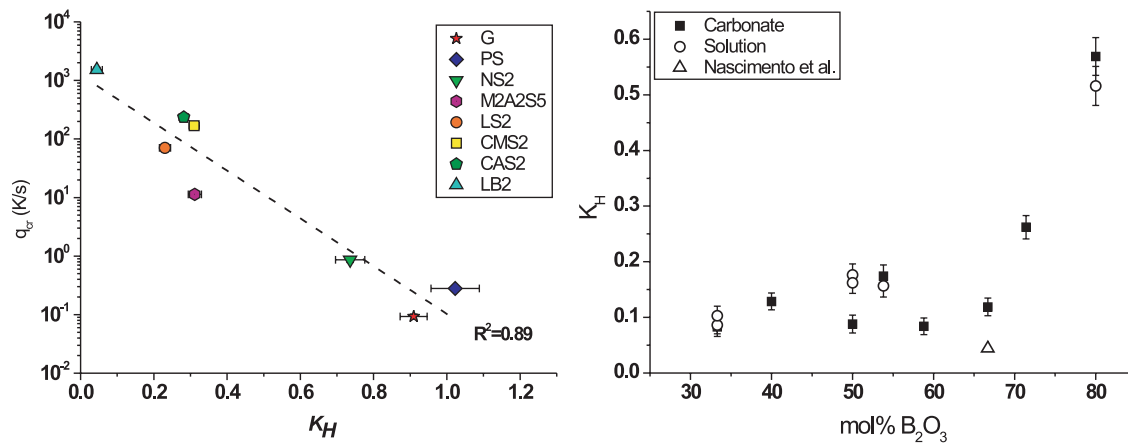


Fig. 12. Left: critical cooling rate⁴ versus the glass stability parameter $K_H = (T_x - T_g) / (T_m - T_x)$ for several compositions. Right: Glass stability parameter K_H versus composition in the Li_2O – B_2O_3 system.

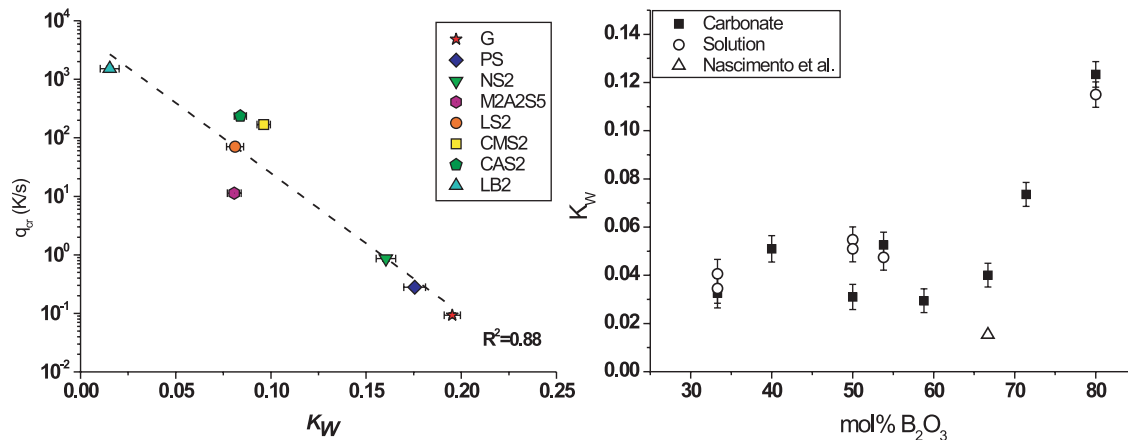


Fig. 13. Left: critical cooling rate⁴ versus the glass stability parameter $K_W = (T_x - T_g) / T_m$ for several compositions. Right: Glass stability parameter K_W versus composition in the Li_2O – B_2O_3 system.

depend on the DSC crystallization temperature (T_x or T_c), this technique is not good for glass-forming compositions for which a crystallization peak cannot be determined during a DSC experiment. We thus confirmed here the findings of Ref. [4] that GS parameters that do not take crystallization peaks into account (K_T and K_1) do not correlate with GFA. Consequently, the range of application of the present technique does not include conventional glasses—very good glass

formers—that are designed not to crystallize during the fabrication process or during a non-isothermal DSC run.

The resulting GS parameters for the present Li_2O – B_2O_3 compositions are shown in the right hand side of Figs. 11–19. One can see that among the compositions for which both the carbonate and solution methods were used (R0.25, R0.86, R1.0 and R2.0), only for R1.0, the GS of glasses prepared by both methods disagree beyond the error limits. This result

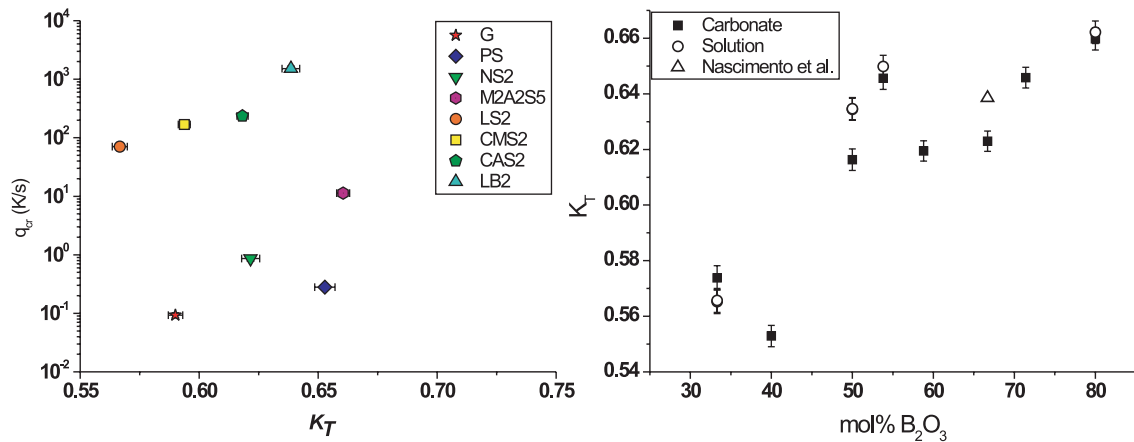


Fig. 14. Left: critical cooling rate⁴ versus the glass stability parameter $K_T = T_g/T_m$ for several compositions. Right: Glass stability parameter K_T versus composition in the $Li_2O-B_2O_3$ system.

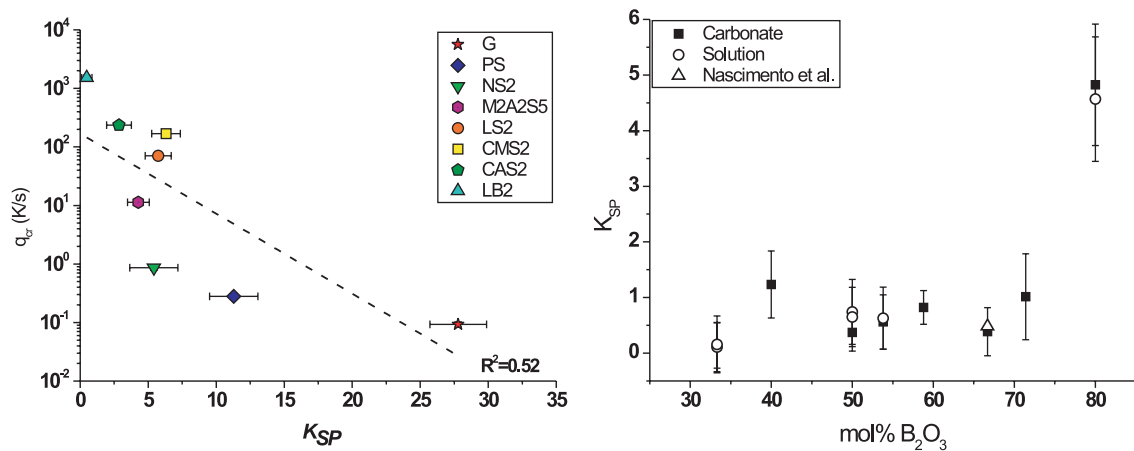


Fig. 15. Left: critical cooling rate⁴ versus the glass stability parameter $K_{SP} = (T_x - T_g)(T_c - T_x)/T_g$ for several compositions. Right: Glass stability parameter K_{SP} versus composition in the $Li_2O-B_2O_3$ system.

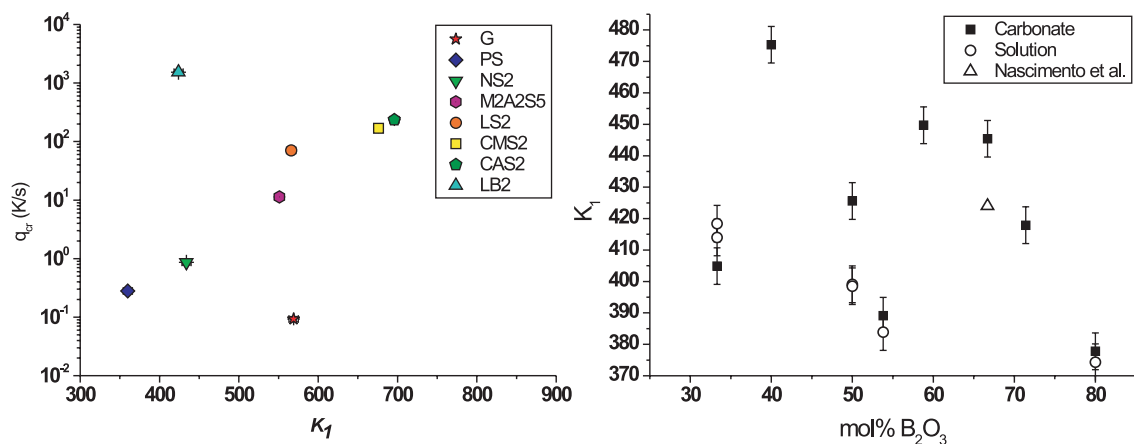


Fig. 16. Left: critical cooling rate⁴ versus the glass stability parameter $K_1 = (T_m - T_g)$ for several compositions. Right: Glass stability parameter K_1 versus composition in the $Li_2O-B_2O_3$ system.

indicates that such discrepancy was due to some uncontrolled experimental variation, and not due to the method of sample preparation. For the other three compositions, the synthesis technique did not significantly affect the thermal behavior of the glasses. If there is some significant difference in the water content in the samples made by the different preparation methods, it is approximately constant and resulted in similar effects in the calculated GS parameters.

Based on the weight loss measurements, there is a small error (a few percent) in the mol% B_2O_3 values, due to small

deviations of the actual glass composition from the nominal one caused by impure chemicals or components lost during weighing, mixing, or melting (see, e.g., the result for the sample with the composition of $Li_2O \cdot 2B_2O_3$ (R0.5), which approaches more the average data if one considers mol% B_2O_3 is deviated a little from stoichiometric composition. Indeed, a melting signal at $806^\circ C$ is observed in the DSC path of the sample R0.5 (detail of Fig. 4). From the PED shown in Fig. 1, for small deviations from the stoichiometric composition ($R = 0.5$), there is a eutectic reaction at $832^\circ C$

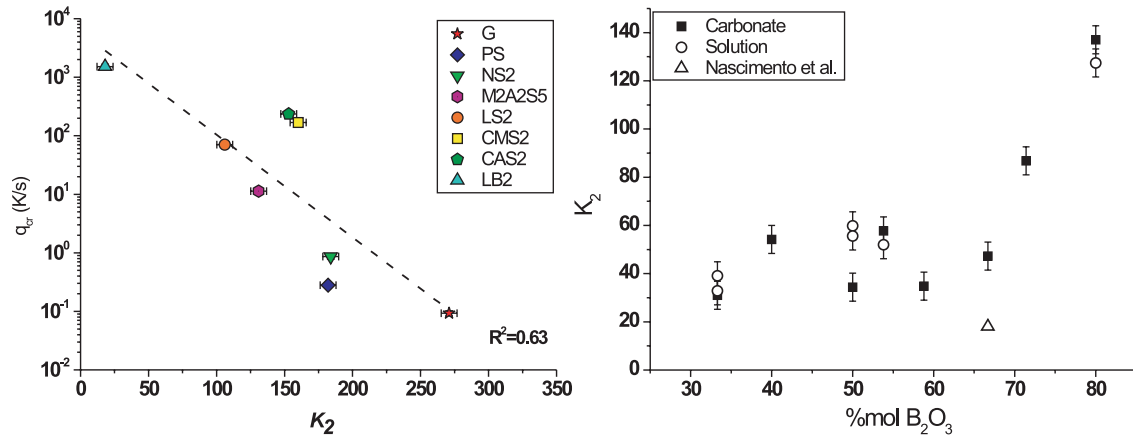


Fig. 17. Left: critical cooling rate⁴ versus the glass stability parameter $K_2 = (T_x - T_g)$ for several compositions. Right: Glass stability parameter K_2 versus composition in the $Li_2O-B_2O_3$ system.

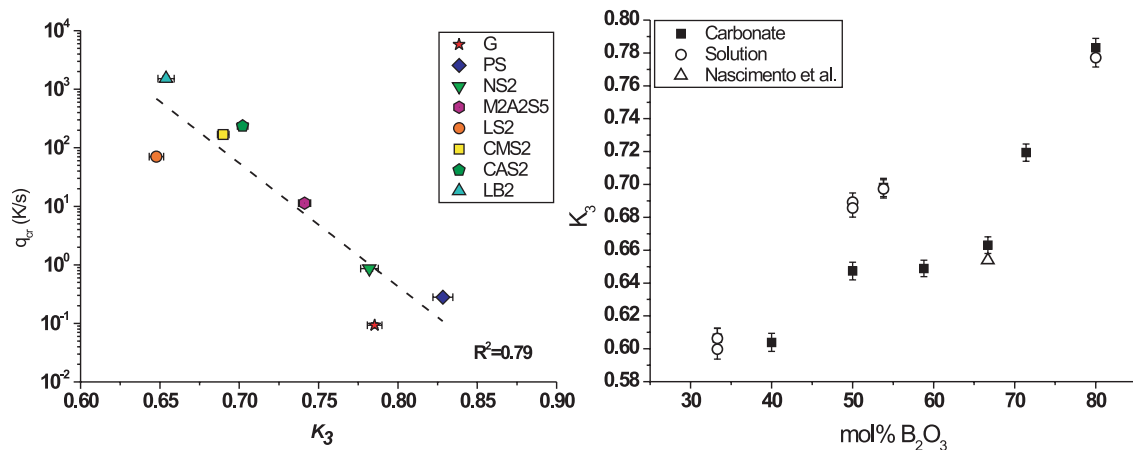


Fig. 18. Left: critical cooling rate⁴ versus the glass stability parameter $K_3 = T_x/T_m$ for several compositions. Right: Glass stability parameter K_3 versus composition in the $Li_2O-B_2O_3$ system.

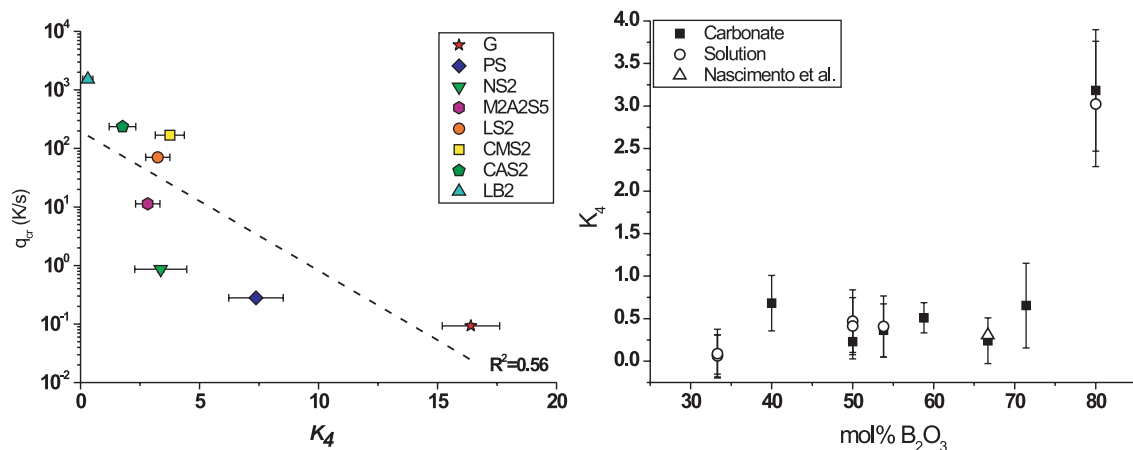


Fig. 19. Left: critical cooling rate⁴ versus the glass stability parameter $K_4 = (T_x - T_g) \cdot (T_c - T_x)/T_m$ for several compositions. Right: Glass stability parameter K_4 versus composition in the $Li_2O-B_2O_3$ system.

for compositions for which $R > 0.5$, and at 856°C for compositions for $R < 0.5$. Assuming that the small melting peak observed at 806°C approaches more the eutectic at 832°C, this indicates a deviation from the nominal composition ($R = 0.5$) toward higher values of R , and thus the resulting approximation of such data point to the average data tendency corroborates our argument.

Taking into account, only the GS parameters that show a good correlation with q_{cr} , the compositions from R2.0 to

R0.7 (i.e., with increasing B_2O_3 from ~33 to 59 mol% B_2O_3) show, in general, the lowest GS values of the scale (given by the corresponding figures in the left) and they are not much affected by the variation in composition indicating poor and invariable GFA in this composition range. However, for glasses with higher B_2O_3 contents (R0.5 to R0.25, or approximately from 67 to 80 mol% B_2O_3), one observes a faster increase of GS, increasing the GFA of the corresponding compositions, as expected

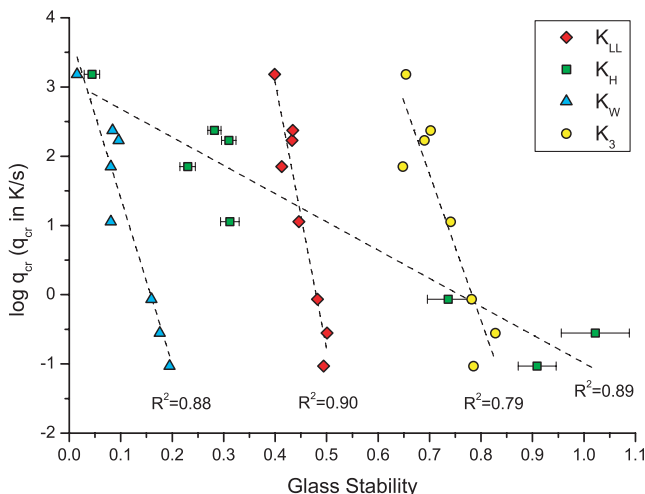


Fig. 20. Comparison of different glass stability parameters, showing that K_H varies in a wider range than K_{LL} , K_W , and K_3 . Error bars for K_{LL} , K_W , K_3 , and $\log(q_{cr})$ are smaller than the data points.

from our qualitative laboratory observations during glass preparation.

Figure 10 shows a minimum in the GS estimated by the Hruby parameter, K_H , for example, which coincides with the maximum liquidus temperature, T_m , within the studied compositional range of the $\text{Li}_2\text{O}-\text{B}_2\text{O}_3$ equilibrium diagram. The GS parameter, K_H , increases as the B_2O_3 fraction increases. However, a secondary maximum in K_H can be observed approximately at the eutectic composition ($R = 0.86$), agreeing with the common sense that eutectic compositions have higher GFA than the other compositions nearby, for the same system. It is possible to admit a secondary maximum in GS for some correlation with composition in the right hand side of Figs. 11–19, at $\sim 50\text{--}54$ mol% B_2O_3 .

One might ask how does the structure of these Li-borate glasses change within the two interesting compositional ranges, i.e. $R = 0.25\text{--}0.50$ (large changes in GS) and $R = 0.50\text{--}2.0$ (only a broad maximum, small changes in the GS parameters).

The structure undergoes a number of changes. First, N_4 (the fraction of tetrahedral borons) increases from 0 at B_2O_3 and reaches a peak of about 0.4–0.5 near $R = 0.4\text{--}0.5$. After that, the borate units revert to trigonal borons with one-two, and finally, three non-bridging oxygens (NBOs) per boron at the expense of tetrahedral borons. N_4 reaches 0 near $R = 2$. Addition of the NBOs ($R > 1/2$) coincides with the region where glass formation becomes more difficult. The limit of glass formation is near $R = 2.8$ or approaching lithium orthoborate ($R = 3$) composed of isolated BO_3 triangles. There is also evidence of intermediate order in the form of boroxol rings ($R = 0$, all borons trigonal and with all bridging oxygens), pentaborate groups ($R = 0.2$ with four boron triangles all bridging oxygens and one tetrahedral boron on two connected rings), triborate rings ($R = 1/3$ six membered ring with two trigonal borons, all bridging oxygens and one tetrahedral boron), diborate groups ($R = 1/2$ with 2 trigonal and 2 tetrahedral borons with all bridging oxygens per unit), metaborate chains and rings ($R = 1$), pentaborate groups ($R = 2$), and the orthoborate isolated units ($R = 3$).^{12,19}

After $R = 0.5$ (33.3 mol% Li_2O), non-bridging oxygen formation tends to steadily depolymerize the network. So long as a covalent network can be formed, the GFA remains significant. As R approaches 0.3, the GFA ends gradually. This is consistent with Figs. 11–19.

We, thus, found that seven stability parameters give similar trends of GS with composition from $R = 0.25$ to $R = 0.5$. Then, GS is approximately constant for a wide range of compositions from $R = 0.5$ (33.3 mol% lithia) to $R = 2$

(66.7 mol% lithia) indicating that, surprisingly, composition does not significantly affect the GFA in this wide compositional range. This general finding qualitatively agrees with our successful experience of preparing the present glasses with compositions up to and including²⁰ $R = 2.8$ (74 mol% lithia) and corroborates the adequacy of simple DSC tests to comparatively gauge the GS and GFA of glasses.

IV. Conclusions

The results reported herein with a series of lithium borate glasses of widely varying composition indicate that several stability parameters, which are relatively simple to measure with a differential scanning calorimeter (DSC), can be used to gauge GS and vitrification ability as a function of composition. Only $K_T = T_g/T_m$ and $K_1 = (T_m - T_g)$, which do not take DSC crystallization peaks into account, are unable to indicate trends of GS with composition; all the other parameters give a similar reasonable trend.

For this particular glass-forming system, seven stability parameters plus laboratory observations during glass preparation indicate that the GFA is more or less the same over a very wide compositional range, from 33 to 67 mol% B_2O_3 . But GFA is significantly augmented with B_2O_3 content for compositions having more than 67 mol% B_2O_3 .

References

- E. D. Zanotto and F. A. B. Coutinho, "How Many Non-crystalline Solids Can Be Made from All THE Elements of the Periodic Table?" *J. Non-Cryst. Solids*, **347** [1–3] 285–8 (2004).
- D. R. Uhlmann, "A Kinetic Treatment of Glass Formation," *J. Non-Cryst. Solids*, **7** [4] 337–48 (1972).
- Sheng Guo, Z. P. Lu, and C. T. Liu, "Identify the Best Glass Forming Ability Criterion," *Intermetallics*, **18** [5] 883–8 (2010).
- M. L. F. Nascimento, L. A. Souza, E. B. Ferreira, and E. D. Zanotto, "Can Glass Stability Parameters Infer Glass Forming Ability?" *J. Non-Cryst. Solids*, **351** [40–42] 3296–308 (2005).
- Z. P. Lu and C. T. Liu, "A New Glass-Forming Ability Criterion for Bulk Metallic Glasses," *Acta Mater.*, **50** [13] 3501–12 (2002).
- Z. P. Lu and C. T. Liu, "Glass Formation Criterion for Various Glass-Forming Systems," *Phys. Rev. Lett.*, **91** [11] 115505 (2003).
- A. Hruby, "Evaluation of Glass-Forming Tendency by Means of DTA," *Czech. J. Phys.*, **22** [11] 1187–93 (1972).
- M. C. Weinberg, "Assessment of Glass Stability Criteria," *Phys. Chem. Glasses*, **35**, 119–23 (1994).
- D. Turnbull, "Under What Conditions Can a Glass Be Formed?" *Contem. Phys.*, **10** [5] 473–88 (1969).
- M. Saad and M. Poulain, "Glass Forming Ability Criterion," *Mater. Sci. Forum*, **19–20**, 11–8 (1987).
- E. I. Kamitsos, A. P. Patsis, M. A. Karakassides, and G. D. Chryssikos, "Infrared Reflectance Spectra of Lithium Borate Glasses," *J. Non-Cryst. Solids*, **126** [1–2] 52–67 (1990).
- E. I. Kamitsos, M. A. Karakassides, and G. D. Chryssikos, "A Vibrational Study of Lithium Borate Glasses with High Li_2O Content," *Phys. Chem. Glasses*, **28** [5] 203–9 (1987).
- S. Feller, W. J. Dell, and P. J. Bray, " ^{10}B NMR Studies of Lithium Borate Glasses," *J. Non-Cryst. Solids*, **51** [1] 21–30 (1982).
- G. D. Chryssikos, E. I. Kamitsos, and M. A. Karakassides, "Structure of Borate Glasses. II: Alkali Induced Network Modifications in Terms of Structure and Properties," *Phys. Chem. Glasses*, **31** [3] 109–16 (1990).
- J. Banerjee, G. Ongie, J. Harder, T. Edwards, C. Larson, S. Sutton, A. Moeller, A. Basu, M. Affatigato, S. Feller, and M. Kodama, "A Solution Approach to High Alkali Content Borate Glasses," *Phys. Chem. Glasses: Eur. J. Glass Sci. Technol., Part B*, **47** [4] 328–31 (2006).
- B. S. R. Sastry and F. A. Hummel, "Studies in Lithium Oxide Systems: V, $\text{Li}_2\text{O}-\text{Li}_2\text{O}_3$," *J. Am. Ceram. Soc.*, **42** [5] 216–8 (1959).
- E. B. Ferreira, M. L. Lima, and E. D. Zanotto, "DSC Method for Determining the Liquidus Temperature of Good Glass-Forming Systems," *J. Am. Ceram. Soc.*, **93** [11] 3757–62 (2010).
- A. F. Kozmidis-Petrovic, "Theoretical Analysis of Relative Changes of the Hruby, Weinberg, and Lu-Liu Glass Stability Parameters with Application on Some Oxide and Chalcogenide Glasses," *Thermochim. Acta*, **499** [1–2] 54–60 (2010).
- S. Kroeker, P. Aguiar, A. Cerqueira, J. Okoro, W. Clarida, J. Doerr, M. Olesiak, G. Ongie, M. Affatigato, and S. A. Feller, "Alkali Dependence of Tetrahedral Boron in Alkali Borate Glasses," *Phys. Chem. Glasses: Eur. J. Glass Sci. Technol., Part B*, **47** [4] 393–6 (2006).
- M. Shibata, C. Sanchez, H. Patel, J. Stark, S. Feller, G. Sumcad, and J. Kasper, "The Density of Lithium Borate Glasses Related to Atomic Arrangements," *J. Non-Cryst. Solids*, **85** [1–2] 29–41 (1986). □